Journal Pre-proof

Catalytic thermal decomposition of the fungicide chlorothalonil and derivatives over different modified zeolites and metal surfaces

María Victoria Cooke, Guadalupe Firpo, Elba Nahir Ruiz Pereyra, Eliana Diguilio, Gustavo Alejandro Argüello, María Soledad Renzini, Walter José Peláez
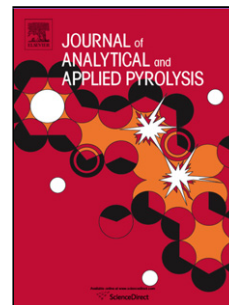
This is a PDF file of an article that has undergone enhancements after acceptance, such as the addition of a cover page and metadata, and formatting for readability, but it is not yet the definitive version of record. This version will undergo additional copyediting, typesetting and review before it is published in its final form, but we are providing this version to give early visibility of the article. Please note that, during the production process, errors may be discovered which could affect the content, and all legal disclaimers that apply to the journal pertain.

Catalytic thermal decomposition of the fungicide chlorothalonil and derivatives over different modified zeolites and metal surfaces.

María Victoria Cooke,[a] Guadalupe Firpo,[a] Elba Nahir Ruiz Pereyra,[a] Eliana Diguilio,[b] Gustavo Alejandro Argüello,[a] María Soledad Renzini[b]* and Walter José Peláez.[a]*

[a]*INFIQC – CONICET – Departamento de Físico Química, Facultad de Ciencias Químicas, Universidad Nacional de Córdoba, X5000HUA Córdoba, Argentina.*
[b]*CITEQ – CONICET – Universidad Tecnológica Nacional, Facultad Regional Córdoba, X5000HUA Córdoba, Argentina.*

*Corresponding author: Dr. Walter J. Peláez – E-mail: waldemar31@fcq.unc.edu.ar. Co-corresponding author: Dra. Soledad Renzini – E-mail: soledadrenzini@gmail.com

Dedicated to the memory of Prof. Gloria Inés Yranzo (1957 - 2008) on the 10th anniversary of her passing.

Graphical abstract

Highligthts

- -Static Gas Phase Pyrolysis of fungicide Chlorothalonil and its derivatives yield mainly dehalogenated compounds and coke.

- -Homogeneous and Heterogeneous reactions (over Fe or Cu wires, H-ZSM-11 and (H/Fe/Cu)-Y Zeolites) have been explored.

- -Pyrolysis products at temperatures higher than 300 ºC were identified through NMR, IR and GC-MS.

- -H-Y zeolite as well as Cu wires proved to be Reusable Catalysts for thermal decomposition of chlorothalonil.

Abstract

Homogeneous and heterogeneous gas-phase static thermolysis of chlorothalonil (CT, **1**) and four derivatives are presented. After thermal decomposition, many interesting products are formed. Chlorothalonil yielded principally carbonaceous residues and dehalogenated compounds, while all the derivatives also afforded a condensed dihydrophenazine (**17**). Relevant information from pyrolysis states that: CT is quantitatively decomposed when compared to its aromatic derivatives; in all cases some potential toxic compounds (which were detected with the help of NMR, GC-MS and IR) are produced; the best catalysts to perform the

decomposition are the acidic zeolite H-Y and metallic Cu; the two zeolites used, (H-ZSM-11 and H-Y) are able to adsorb the substrates, but only H-Y is capable of decomposing CT in carbonaceous residues.

Keywords

-Gas Phase Pyrolysis

-Organochlorine fungicide derivatives

-Heterogeneous decompositions

-Zeolites

-Reversible deactivation

1. Introduction

Chlorothalonil (CT, **1**) is a broad-spectrum non-systemic organochlorine fungicide generally used both in the prevention and control of fungal diseases.[1] It is classified as type IV fungicide, usually causing no harm when applied as indicated for each crop. Nevertheless, the damage caused by residual fungicide through bioaccumulation is still unknown. Besides, it has been classified as a probable human carcinogen.[2]

Very recently, we have published a paper dealing with the photodegradation mechanism of **1**. That study afforded new insights on photoproducts that were not reported before. Also a comprehensive discussion of the UV spectrum as well as the vibrationallly resolved HOMO-LUMO transitions were reported for the first time.[3]

In the present contribution we deal with thermal studies of **1** and some of its derivatives, namely 2,4,5-trichloro-6-((2-chloroethyl)amino)isophthalonitrile (CTC, **2**), 2,4,5-trichloro-6-(phenylamino)-isophthalonitrile (CTAn, **3**), 2,4,5-trichloro-6-((4-chlorophenyl)amino)isophthalonitrile (CTClAn, **4**) and 4-((4-bromophenyl)amino)-2,5,6-trichloroisophthalonitrile (CTBrAn, **5**), **figure 1**. The gas-phase thermal reactions were performed both homo- and heterogeneously. Solid catalysts (zeolites H-ZSM-11 and H-Y, their metal modified derivatives as well as metallic wires of Cu and Fe) were used, in an attempt to close the gap on the knowledge for the ultimate fate of **1** in the environment. New efforts aimed to analyze and comprehend the reactions lead us to perform a thorough analysis on solid catalysts (i.e. zeolites and metal surfaces) to assess whether they are suitable either to adsorb or decompose these contaminants.
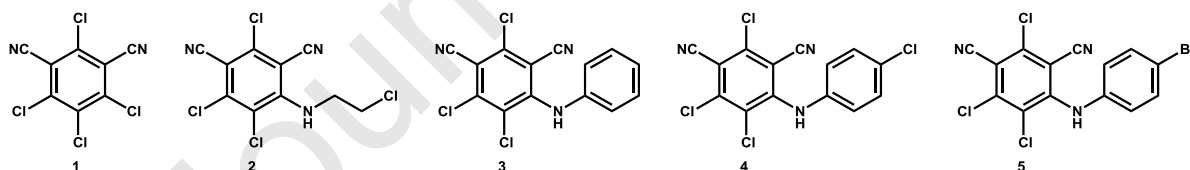
Figure 1. Chemical structures of Chlorothalonil (**1**) and its aliphatic (**2**) or aromatic (**3-5**) derivatives prepared by Microwave synthesis and pyrolyzed in this work.

Zeolites are crystalline microporous aluminum-silicates with various structures having intrinsic properties as strong acidity, high surface area, high thermal stability and shape selectivity, thus rendering a great number of applications in the field of petrochemical and fine chemical processes.[4,5,6] However, the existence of micropores in zeolites often imposes significant limitations. Among them, it can be mentioned the formation of coke in the pore structure, which leads to a progressive decrease of the zeolite activity.[7] This deactivation is mainly due to the trapping of products from secondary reactions (heavy organic compounds) within the micropores, which can either poison the

active sites or block the accessibility to reactant molecules. The regeneration of zeolite catalysts requires the removal of coke, a task achieved by simple oxidative treatment at high temperatures.

It is the main objective of this work to investigate the thermal and catalytic decomposition of the fungicide chlorothalonil and derivatives. For this purpose, the results obtained using metallic surfaces and microporous zeolites ZSM-11 and Y, both, in their protonic and metallic forms, will be presented.

2. Materials and methods

2.1. General

Chlorothalonil **1** was obtained from a commercial source (Adama S.A., Odeón 82, 82.5%). It was purified by column chromatography using hexane, hexane/dichloromethane (80:20) and dichloromethane to give **1** as a white solid (>99% purity, mp: 250-252°C, lit. mp: 250-251°C).[8] The purity was checked by IR, GC-MS and (^{13}C) NMR spectroscopy, see **figures S1-5** in the Supplementary Material (**S.M.**).

Static homogeneous pyrolyses were performed inside a tube furnace with a temperature-controller device. The substrate (25 mg, 0.1 mmol), before going into the furnace, was introduced in the glass reactor (1.5 x 12 cm Pyrex), then cooled in liquid nitrogen in order to evacuate all the remaining gases, sealed under vacuum (0.06 mbar) and finally placed in the furnace and heated for 10-30 minutes at 300-400°C. For the reactions in the presence of zeolites, that is for the heterogeneous reactions, the substrate and the zeolite were introduced in the reaction tube using a 1:1 weight proportion (25, 50 or 100 mg in total). For the reactions in presence of metal surfaces, approximately 2.0 g of either iron or copper wires of 3.0 cm of length and 0.25 mm of diameter and previously washed with HCl (0.1M), were introduced in each reactor, and then the substrate was added. After appropriate vacuum and sealing, the samples were heated at 300°C during 10-30 minutes.

Irrespective of the type of reaction, all the products as well as the unreacted reagent and catalyst remained together for the whole time of the reaction. In all cases, the resulting pyrolizates were extracted with 5mL of ethyl acetate. In the case of heterogeneous reactions, a Nylon filter (Sigma, 0.22 micron pores) was used to separate the organic soluble phase from the catalyst employed. Both fractions were dried and weighed to calculate the mass remained percentage in the organic phase (%m_{rem}, equation 1) and the mass adsorbed for the different materials (%m_{ads}, equation 2), where m_i is the initial mass of CT at the beginning of the reaction.

$$\%m_{rem} = \frac{m_{rem}}{m_i} x100 \qquad \text{Equation 1}$$

$$\%m_{ads} = \frac{(m_i-m_{rem})}{m_i} x100 \qquad \text{Equation 2}$$

It is important to note that no gas production was observed in the heterogeneous reaction of CT. All the organic soluble phases were analyzed via GC-MS to determine the amount of CT remainder and the formed dehalogenated products. On the other hand, after the pyrolysis reactions all zeolites were analyzed by FTIR and TGA (Bruker IFS28 FTIR and Shimadzu DTG-60 analyzer). This allow us to propose that carbonaceous residues were formed within the zeolites channels, that remain together with few amount of unreacted CT (also see TGA **figures S40-47** in the Supplementary Material). Scanning Electron Microscopy (SEM) was performed using a Zeiss Sigma field-emission gun electron microscope for determination of morphology, particle size and surface chemical composition of zeolites.

2.2. CT derivatives

2,4,5-trichloro-6-((2-chloroethyl)amino)isophthalonitrile (CTC, **2**), 2,4,5-trichloro-6-(phenylamino) isophthalonitrile (CTAn, **3**), 2,4,5-trichloro-6-((4-chlorophenyl)amino)isophthalonitrile (CTClAn, **4**) and 4-((4-bromophenyl)amino)-2,5,6-trichloroisophthalonitrile (CTBrAn, **5**), were prepared by modifying a procedure described in the literature.[9] In

our case, we employed Microwave induced reactions as a greener methodology, and got better yields with shorter reaction times. More detailed description of the method is presented in the supplementary material (see **Tables S1** and **S2**).

2.3. Synthesis of Catalysts

The catalysts employed were ZSM-11 (MEL) and Y (FAU) zeolites. ZSM-11 was synthesized by means of the hydrothermal crystallization method using tetrabutylammonium hydroxide (TBAOH, Fluka) as directing agent.[10] Zeolite Y was provided by Aldrich. The ammonium forms of the zeolites were prepared by ion exchange of the as prepared Na-zeolite form with 1 M ammonium chloride solution at 80°C for 40 h. Thermal treatment under nitrogen flow for 8 h at 500°C and then calcination in air at the same temperature for 10 h yielded finally the zeolites.

Transition metals were incorporated in the zeolite matrix by the wet impregnation method. For this purpose, the ammonium form of the zeolite was suspended in an aqueous solution of the proper salt: $FeCl_2 \cdot 4H_2O$ (Mallinckrodt), for Fe-Y and $Cu(C_2H_3O_2)_2 \cdot H_2O$ (Mallinckrodt), for Cu-Y. The water was evaporated using a rotator−evaporator at 80°C under vacuum until complete dryness. Then samples were dried at 110°C and desorbed in N_2 flow at 500°C for 12 h, followed by calcination in air at 500°C for 8 h to obtain the M-Y samples.

2.4. Characterization of reactants and products

All compounds were characterized by standard spectroscopic techniques (^{1}H-, ^{13}C- NMR, HMBC, HSQC, UV, IR) and mass spectrometry, and all data are in agreement with the proposed structures. NMRs were recorded in DMSO-d_6 with a Bruker Avance II 400 MHz spectrometer (BBI probe, z gradient) (^{1}H at 400.16 MHz and ^{13}C at 100.56 MHz). Chemical shifts are reported in parts per million (ppm) downfield from TMS. The spectra were measured at 22°C. Infrared solid spectra were recorded with an FTIR Bruker IFS 28v spectrometer, with a resolution of 2 cm^{-1} in the range from 4000 to 400 cm^{-1} by using KBr disks. Gas chromatography/mass spectrometry (GC/MS) analyses were performed with a Shimadzu GC-MS-QP 5050 spectrometer equipped with a VF column (30 m x 0.25 x mm x 5 μm) by using helium as eluent at a flow rate of 1.1 mL min^{-1}. The injector and ion source temperature was 280°C, the oven heating ramp was 15°C min^{-1} from 150 up to 280ºC for **1** and from 200 up to 280ºC for **2-5**, and the interface temperature was 280°C. The pressure in the MS instrument was 10^{-5} Torr, precluding ion-molecule reactions from taking place, and MS recordings were made in the electron ionization mode (EI) at ionization energy of 70 eV. Quantification of chlorothalonil **1** remaining was performed via GC using chlorothalonyl supplied by Riedel-de Haen (99.2%) as standard. Through GC it was possible to obtain a relative profile of the disappearance of CT and the appearance of the different products. Although a total isolation of the pyrolysis products were not achieved by preparative chromatography, the analysis of the ^{1}H-NMR and the GC-MS spectra of the different reactions allowed us to identify several isomers of the products. Full characterization of chlorothalonil **1**, and its derivatives **2-5** are presented in the **S.M.** (see **figures S6-25**).

2.5. Characterization of catalysts

The catalysts were characterized by different techniques. The Si, Al, Cu and Fe content of the zeolites were determined by inductive coupled plasma spectroscopy (ICP) in a Varian 715ES. X-ray powder diffraction (XRD) patterns were collected in air at room temperature on a Phillips PW-1700 equipment, using Cu Kα radiation of wavelength 1.54 Å. Diffraction data were recorded from 5° to 60° 2θ angles, with an interval of 0.01° and a scanning speed of 2°/min. See XRD patterns of zeolites H-Y and H-ZSM-11 in the **S.M.** (**figure XRD1**). The assessment of the specific surface areas by the BET method was carried out with N_2 adsorption at 77 K using Micromeritics ASAP 2000 equipment. Infrared measurements on the zeolites were performed in a JASCO 5300 FTIR spectrometer. For the structural characterization in the lattice vibration region (400−1800 cm^{-1}), the samples were mixed with KBr at 0.05% and pressed to form wafers. To determine the type and concentration of acidic sites, pyridine (Py) adsorption

experiments were carried out on self-supporting wafers (8−10 mg/cm^2) of the zeolites using a thermostatted cell with CaF$_2$ windows connected to a vacuum line. Pyridine (3 Torr) was adsorbed at room temperature and desorbed (10^{-4} Torr) at 250, 350, and 400°C for 1 h. The number of Brönsted and Lewis acid site was calculated from the maximum intensity of the adsorption bands at 1545 and 1450−1460 cm^{-1}, respectively, and quantified using literature data of the integrated molar extinction coefficients, which are independent of the catalysts or strength of the sites.[11] Thermogravimetry experiments in a TGA/SDTA851e/SF/ 1100°C Mettler Toledo thermobalance were performed on the catalysts.

3. Results and Discussion

3.1. Catalysts Characterization

The main physicochemical characterization results of the catalysts under study are summarized in **table 1**. The surface area (S$_{BET}$) of zeolites Y are significantly greater than ZSM-11. Crystallinity, as assessed from both XRD and FTIR techniques is very high, thus confirming that the severe conditions employed during the chemical and thermal treatments did not affect the structural characteristics of the catalysts. The XRD patterns of the H-ZSM-11 and H-Y zeolites show the characteristic signals corresponding to each structure at 2θ = 23-24 and 2θ = 7-9 degrees and 2θ = 6.13, 10.09, 11.91, 15.71, 18.61, 20.41, 23.71, 27.07 and 31.43 degrees, respectively (no diffractograms are presented).

Table 1. Physicochemical properties of zeolites.

Catalyst	Si/Al	Metal Loading (%wt)	Surface area (m^2/g)	Crystallinity (%)	
	ICP	ICP	BET*	XRD	FTIR*
H-ZSM-11	18.01	--	378	100	>99
H-Y	2.41	--	708	>99	>99
Cu-Y	2.30	2.4	602	>99	>98
Fe-Y	2.30	2.8	607	>99	>97

*FTIR in the fingerprint zone of the materials (400-1400 cm^{-1}).

FTIR spectroscopy of pyridine adsorption over acid materials is a common technique to characterize the nature and strength of acid sites. It is based on the observation of the vibrational perturbation that is undergone when this kind of probe-molecules adsorb on them.[12] Pyridine was adsorbed at room temperature over the samples and desorbed at 400°C under vacuum for one hour. Bands at 1455, 1490 and 1545 cm^{-1} can be observed in all zeolites. The band at 1490 cm^{-1} corresponds to the vibration of pyridine adsorbed over Brönsted and Lewis acid sites.[13,14] Bands at 1455 cm^{-1}, corresponding to the interaction with Lewis acid sites (PyL), as well as bands at 1545 cm^{-1}, indicative of the Brönsted interaction (PyH$^+$). The H-ZSM-11 catalyst shows a signal of PyH$^+$ sites at 1545 cm^{-1} and a less important PyL signal resulting from Al^{3+} sites. H-Y exhibits a behavior similar to H-ZSM-11, but presents a major number of total acid sites. The increase of Lewis acid sites after the incorporation of transition metal cations is probably produced by the formation of a new strong electron-donor-aceptor (EDA) adduct of Pyridene-Lewis sites (PyL), **table 2**. The total number of acid sites is bigger for the Y zeolites than the ZSM-11 zeolite, because the Faujasites possess a low Si/Al ratio that means a more significant quantity of Al^{+3} cations and greater deficiency of negative charge in the zeolite framework. A higher number of positive ions is necessary to neutralize the negative

charge of the Y zeolite structure. Besides, the FAU zeolites have bigger pore size than MEL zeolite. For these reasons, FAU catalyst can incorporate a higher number of transition metal cations into their structures and they possess a greater quantity of acid sites than MEL zeolites.

Table 2. Brönsted and Lewis acid sites in FAU and MEL zeolites

Catalyst	Brönsted sites (mmol Py/g)*	Lewis sites (mmol Py/g)*	Total acid sites (mmol Py/g)*	B/L
H-ZSM-11	18.51	2.02	20.53	9.16
H-Y	30.2	2.46	32.66	12.28
Cu-Y	17.20	25.67	42.87	0.67
Fe-Y	28.87	19.56	48.43	1.47

*FTIR results of pyridine adsorbed in zeolites after evacuation at 400°C and 10^{-4} Torr for 1 h.

Magnified images shown in **figure 2** (a: ZSM-11, b: Y, c: Cu-Y and d: Fe-Y) present a very clear and sharp crystallinity for all zeolites.

6
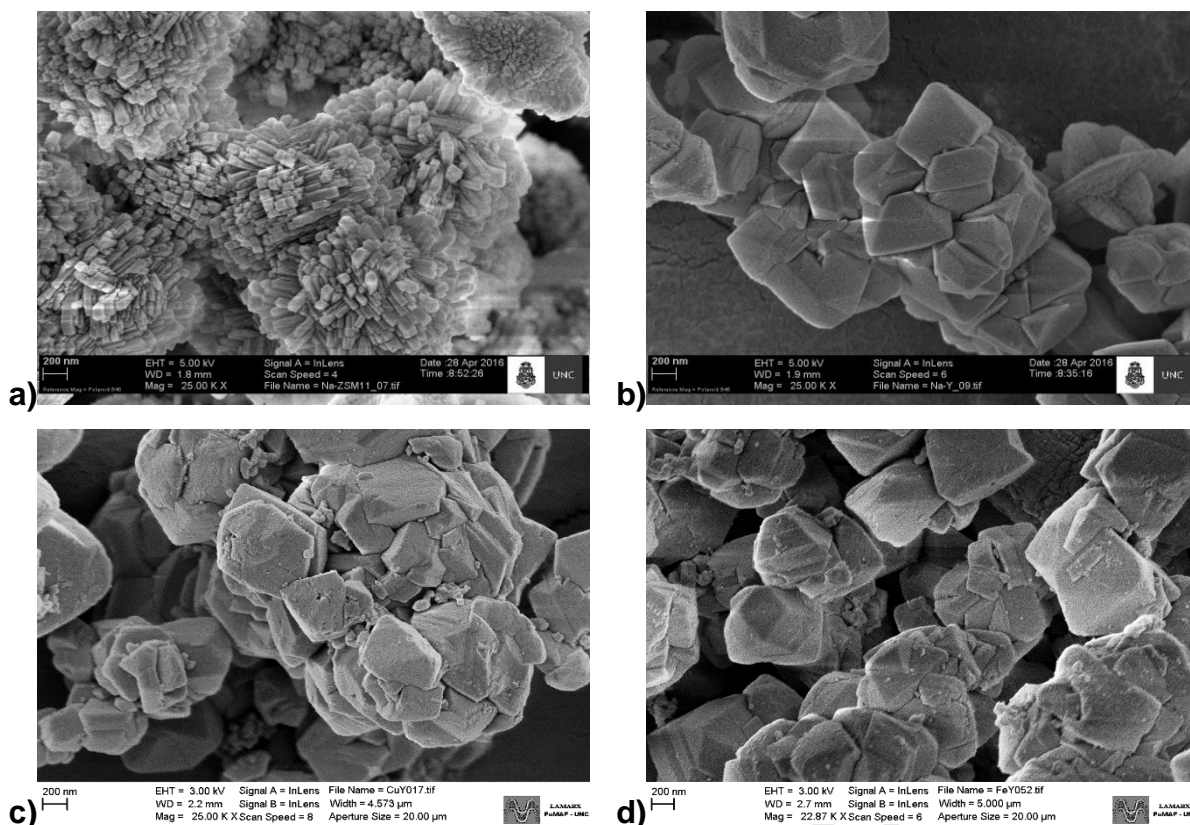
Figure 2. SEM images of zeolites showing the clear and sharp crystallinity. **a)** ZSM-11, **b)** Y, **c)** Cu-Y and **d)** Fe-Y.

3.2. Pyrolysis of chlorothalonil 1 in homogeneous and heterogeneous conditions.

In the homogeneous pyrolysis of **1** at 300ºC and 0.06 mbar for 30 minutes, only the sublimation of the substrate was observed, recovering 100% of the mass (**1** rendered very stable under these conditions). For this reason, the catalytic heterogeneous pyrolysis was studied, using two zeolites with physicochemical different properties and structures: H-ZSM-11 and H-Y (section 3.1). After each pyrolysis, the crude of reaction was extracted with solvent and the percentage of **1** remaining in the organic phase was measured and quantified by GC at different reaction times (10, 20 and 30 min, **figure 3**). In the case of H-ZSM-11, there was not a clear trend in the amounts remaining
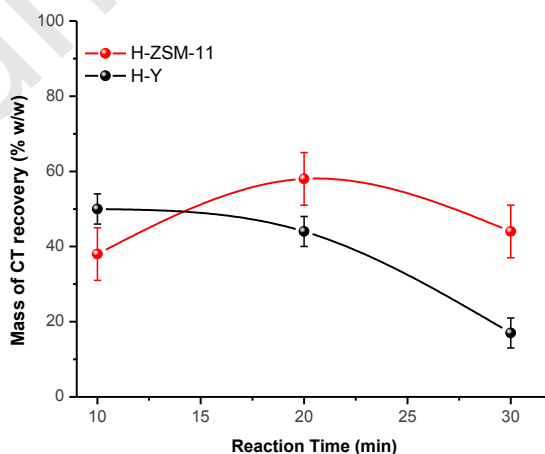
(39-59% of **1**).

Figure 3. Percentage of mass remained (%w/w) of CT (**1**) vs reaction time over H-Y zeolite (-•-)

and H-ZSM-11 zeolite (-•-), **1**:catalyst ratio = 1:1.

On the other hand, for H-Y, there is a marked decrease of mass remaining at longer times (53, 45 and 18%, respectively). This result could be related to either the larger surface area, size of the channels and greater number of acid sites of the H-Y zeolite, which would allow to host and degrade the chlorothalonil molecule. No gas production was observed during these pyrolyses. However, for H-Y, it is evident at first sight, that appreciable amounts of coke are retained within the zeolite. FTIR spectra of the recovered catalysts after different pyrolysis times as well as the aspect of the KBr pellets are shown in **figure 4**. No apparent differences in the main vibrational bands were found which denote that the crystalline structure of the zeolites has not been compromised. Nevertheless, for H-Y, new bands at approximately 1450 cm^{-1} are detected and assigned to the carbonaceous residue trapped within the channels of the zeolite.
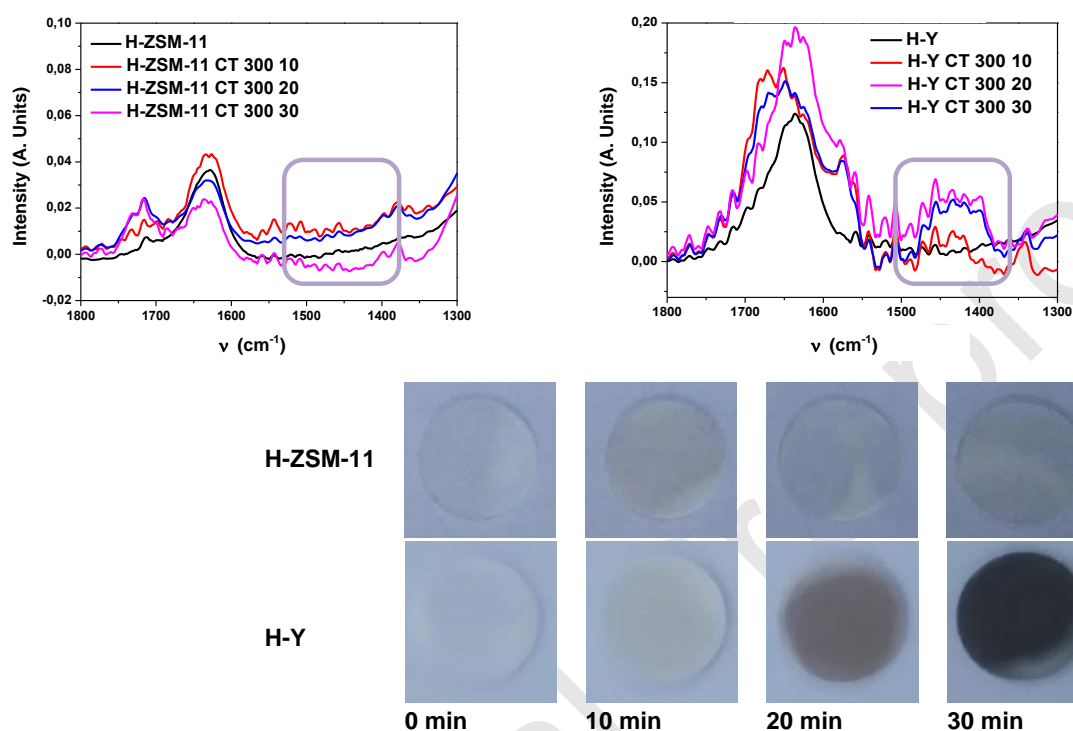
Figure 4. FTIR of a selected region for H-ZSM-11 (up to the left) and H-Y (up to the right) and KBr pellets of the samples at different pyrolysis times. The violet square denotes the carbonaceous residue band within the zeolite.

The TGA of the zeolites after the pyrolysis (performed at different periods) are shown in **figure 5** (see **S.M.** for the TGA of pure **1, figure S5**). In the case of H-ZSM-11 (**figure 5a**), the only significant mass loss comes from desorption of **1** adsorbed within the zeolite (10% of mass loss when the thermolysis are performed for 10 min). Nevertheless, when the thermolysis reaction is performed for longer times (30 min), the amount of **1** absorbed increases (30% of the mass). On the other hand, TGA results for H-Y are far more complex since it entails the decomposition of **1** inside the channels (**figure 5b**).[15] TGA indicates that multi-step decompositions are occurring with low stability of the species formed. The most relevant information from this analysis is that the mass remaining increases with time (from 10 to 30 min).
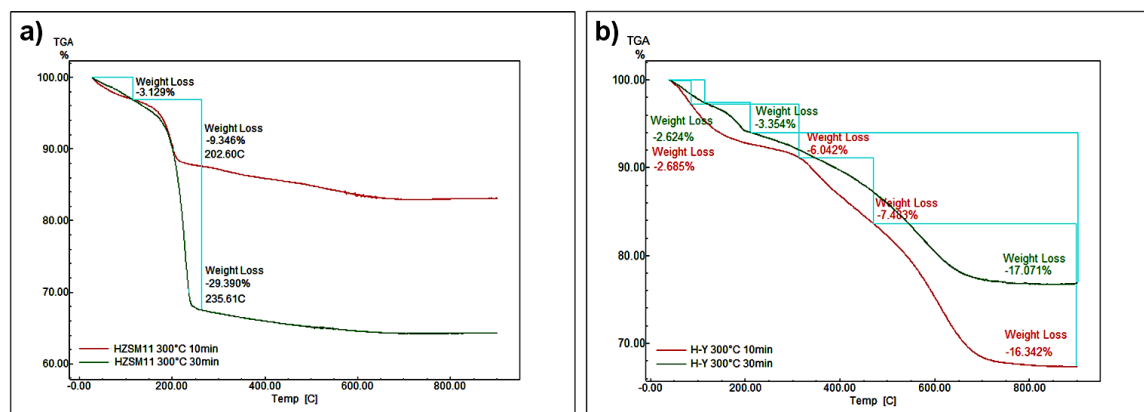
Figure 5. TGA of H-ZSM-11 (**a**) and H-Y (**b**) at different pyrolysis times.

Also, the extracted crude from the reactor was analized *via* GC-MS. **Scheme 1** presents the thermal decomposition products observed for each case. While in homogeneous reaction **1** suffered no decomposition, the same cannot be said for the heterogeneous experiments. The mass remaining corresponds to approximately 50% of the initial total mass for H-ZSM-11 and 20% for H-Y. However, over 95% of it, corresponds to **1**. In both cases the products come from the reductive dechlorination of **1** (compounds **6a-b** and **7a-b**). See **figures S26-29** in the **S.M..**
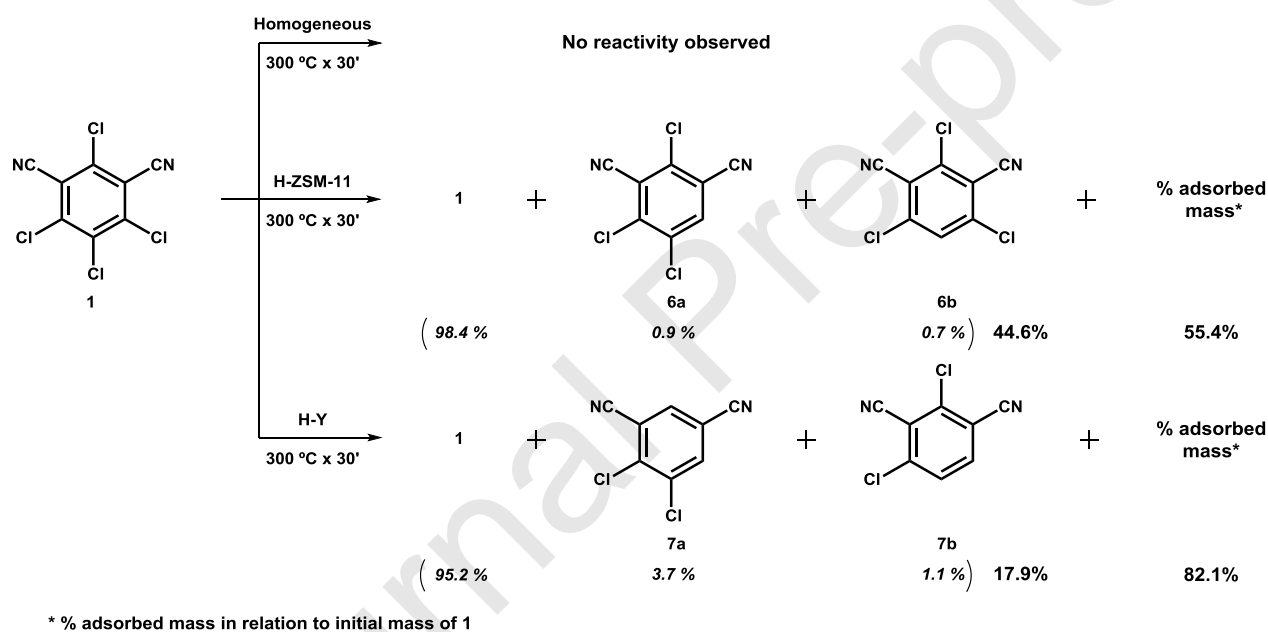
Scheme 1. Homogeneous and heterogeneous pyrolysis of **1** (**1**:catalyst ratio = 1:1).

The H-Y zeolite exhibited better catalytic performance than H-ZSM-11 when decomposing **1**. It was the preferred choice for both, its cost and since it can be commercially obtained.

The effect of the ratio **1**/HY was investigated, carrying out the pyrolysis at 300°C for 5 min. This result is presented in **figure 6a**. Since almost 95% of the mass remaining is **1**, we can infer that the decomposition is practically constant (26-30%) down to a ratio of 1:1; from there, the decomposition increases with the decrease of the ratio **1**/HY.

9

The possibility of recovering and reusing the catalyst was evaluated for H-Y. Thus, the crude of reaction was washed with ethyl acetate, filtered off, dried at room temperature, and the catalyst reused without any calcination treatment, **figure 6b**. The mass remaining obtained after the first cycle of reuse with the catalyst without reactivation (2nd reaction) was slightly higher than the obtained using the fresh catalyst (20% and 17.9%, respectively). Nevertheless, in the 3rd and 4th cycle, the increment was significantly high (32.7% and 45.7%). Therefore, reactivation of the zeolite is proposed every two cycles.
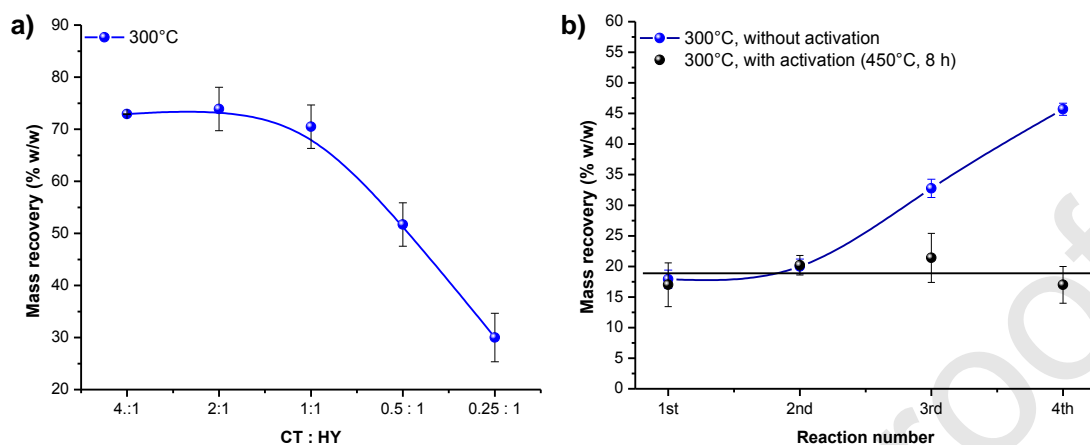
Figure 6. a) Percentage of mass remained (%w/w) vs **1**/HY ratio. **b)** Percentage of mass remaining (%w/w) vs reaction with (-•-) and without (-•-) catalyst activation.

Together with the desired cracking reactions, the formation of coke in the pore structure of the catalysts also occurs and leads to a progressive decrease of the zeolite activity.[16] This deactivation is mainly due to the trapping of organic compounds within the micropores, resulting from secondary reactions and which can either poison the active sites or block the accessibility to reactant molecules.[17] The presence of micropores inhibits facile mass transfer to and from the active sites, leading to a shortening of the useful life. This behavior has been reported by several authors in different catalytic processes.[16,18,19]

Adsorbed products or residues can be removed by an adequate thermal treatment. However, this handling could induce structural changes that would modify the catalytic degradation. In order to study this possibility, new reactions were performed and after the first use, the catalyst was separated by filtration, treated at 450°C for 8h, and reused, **figure 6b**. The **1** degradation value was similar to that obtained with fresh catalyst (2nd reaction, 20% of mass recovered). Analysis of the mass recovered after the 3rd and 4th reactions show that the activity increases compared with the catalyst without activation. Although, for the different reactions, the activity is within the experimental error we would say that the activity was practically completely restored, in spite of the pale dark color of the catalyst which denotes the presence of carbonaceous residues in the zeolite.

The characterization for the fresh and used zeolites were carried out. **Figure 7** shows the XRD patterns at 0 (fresh), 2nd (H-Y*) and 4th (H-Y**) cycles. It can be seen that there are no new diffraction peaks exhibited in the XRD patterns of catalyst used, neither the positions of diffraction peaks change, showing no new phases formed during the activation. However, the intensities decrease, indicating that crystallinity has slightly decreased, probably owing to the deposition of coke at pore mouths of the zeolite catalyst.[20]
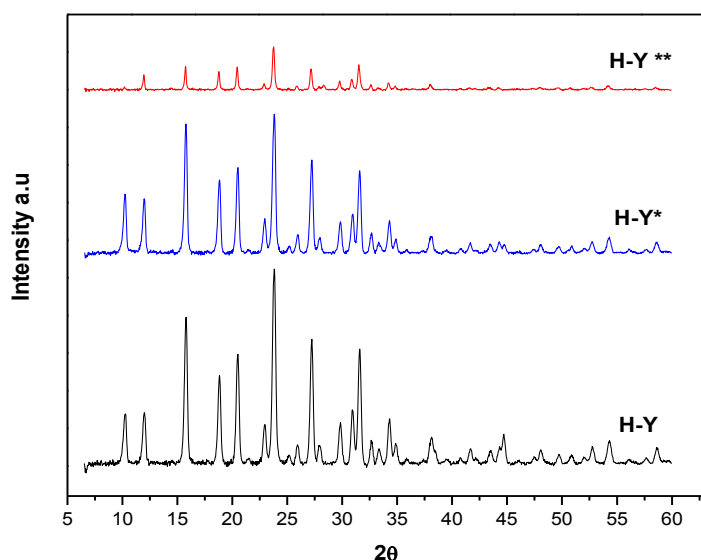
Figure 7. XRD patterns of fresh and used Y zeolite. H-Y (fresh), H-Y* (after 2nd cycle) and H-Y** (after 4th cycle).

3.3. Pyrolysis of *1* with metal surfaces and M-Y zeolites

We have previously reported the efficient decomposition pyrolysis reaction of 2-chloroethyl isocyanate over metal surfaces.[21] Due to the results obtained and the stability of **1**, new pyrolyses over metal surfaces and modified Y zeolites with iron (Fe-Y) or copper (Cu-Y) cations were proposed.

After the pyrolysis, the modified zeolites were analyzed by FTIR, and the spectra showed the presence of coke, **figure 8**. In addition, all pyrolyzates previously extracted with organic solvents were analyzed *via* GC-MS and the decomposition products identified. They come from reductive dechlorinations, decyanations or a combination of both reactions. In particular, Cu provided the higher decomposition of **1** with more than 88% of the mass converted to coke and left adsorbed on the metal surface while Fe only decomposes approximately 32%. In both cases, substrate and other aromatic compounds principally compose the extracted organic phase, as it can be seen in **scheme 2** and MS in the Supplementary Material (**figures S30-36**).

In the reaction over cationic Y zeolites and in opposition to the behavior of the metallic surfaces, the best catalyst was the Fe-Y zeolite. This adsorbs and decomposes approximately 72% of the reactant, while the Cu-Y zeolite only 59%. Here again, the organic extract is compound principally by **1** and the same kind of products previously obtained over metal surfaces. Then, it is important to highlight that the most effective materials for the decomposition of **1** are copper wires and H-Y zeolite.
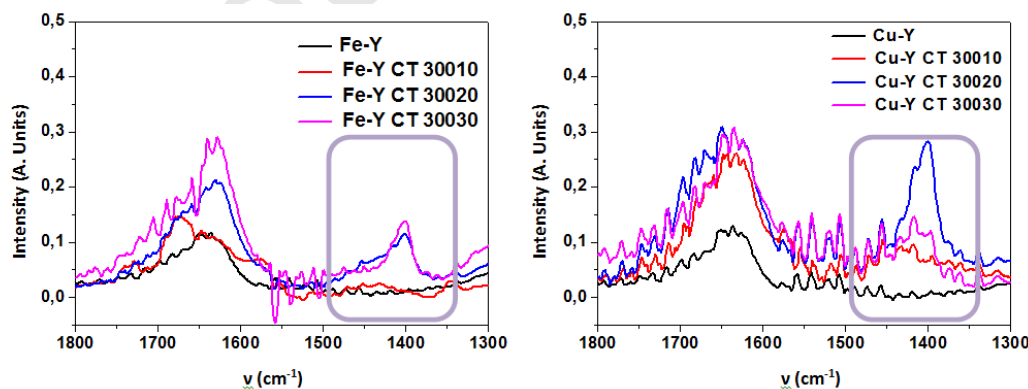
Figure 8. FTIR of Fe-Y (left) and Cu-Y (right) at different pyrolysis time.
The violet square denotes the soot residue band within the zeolite.

* % adsorbed mass in relation to initial mass of 1
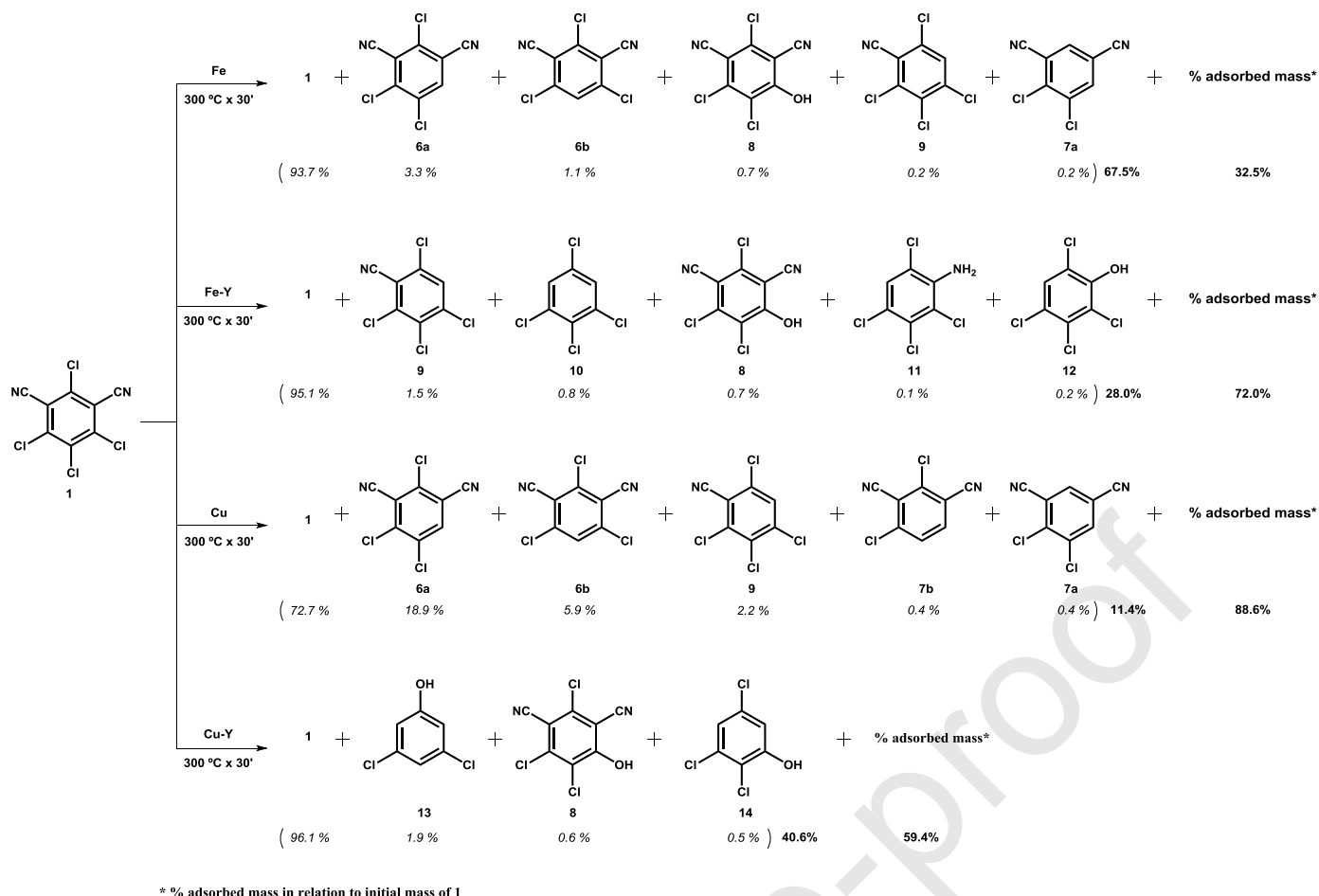
Scheme 2. Heterogeneous pyrolysis of **1** with metal surfaces and cationic Y zeolites.

Zeolites as well as the metal surfaces have presented greater decomposition of **1** than purely thermal pyrolysis. The percentage of mass remaining is presented in **table 3**.

There, remarkable differences between the behavior of metal surfaces and modified zeolites can be observed. For example, in the pyrolysis over metallic wires, the mass remaining over iron is higher than the obtained with copper at any time. Comparing acidic zeolites, processes performed over H-Y produced more decomposition than H-ZSM-11 at 30 min. Nevertheless, in the pyrolysis with modify zeolites, the organic material recovered was higher with Cu-Y than the obtained with Fe-Y.

Table 3. Percentage of mass remaining (%w/w) in the pyrolysis of **1** with metal surfaces and zeolites at 300ºC.

Time (min)	Homogeneous	Metal Surfaces		H-Zeolites		HM-Zeolites	
		Fe	Cu	H-Y	H-ZSM-11	Fe-Y	Cu-Y
10	N.R	45.0	19.2	53.3	-	37.1	40.3
30	99	67.5	11.4	17.9	44.6	28.0	41.0

On the other hand, the Fe-Y and Cu-Y zeolites exhibit a greater number of Lewis acid sites with respect to the zeolites in their protonic forms (as can be seen in **Table 2**). Nevertheless, analyzing the different types of acid sites individually (Brönsted, Lewis or Totals) with respect to the %mass recovered it could be determined that the Brönsted acid sites are those that interact selectively with the CT molecule. To shed some light on these results, normalized catalytic results as a function of the surface area and Brönsted acidic sites of the different materials used are presented in **figure 9a** and **9b**, respectively. As it was observed for other authors,[22] the catalytic degradation increase with the increasing in the surface area, having a linear behavior for some of these solid (Fe < H-ZSM-11 < Fe-Y < H-Y). However, the catalytic behavior for Cu and Cu-Y resulted anomalous to this trend, **figure 9a**. Cu-Y have less catalytic effect in comparison with Fe-Y, which possesses almost the same surface area, oxidation state and metal loading (**Table 1**). A difference for this could be related to the oxidation state of the metals. Nonetheless, L. Ji *et al.* reported the pyrolysis of polyethylene in the presence of iron and copper salts.[23] In that work, it was proved that cationic metal salts improved the efficiency of the decomposition of polyethylene, but the oxidation states of the metals are not the predominant parameter for the slightly increased activity observed of copper (II) over the iron (II) and iron (III). According with these results and acidic sites analysis (through FTIR, **table 2** and **figure 9b**), it is possible to suppose that Brönsted acid sites favor **1** conversion, probably by the selective interaction between substrate molecules and Brönsted acid sites. In addition to this, we suggest that Cu-Y would has been poisoned with carbonaceous residue faster than Fe-Y as it was observed in the IR spectrum in **figure 8** yielding a less catalytic
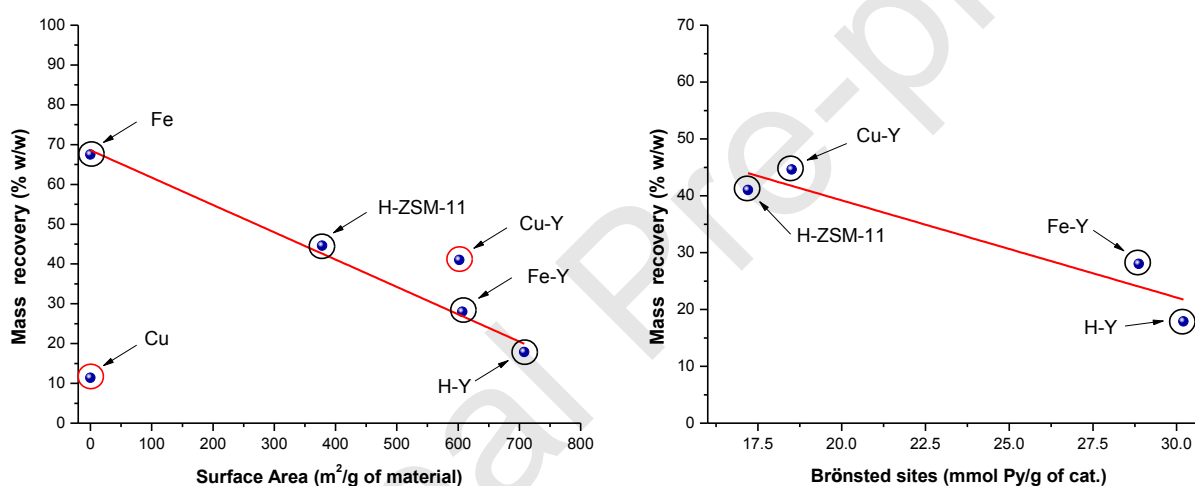
degradation than Fe-Y.

Figure 9. Mass recovery % as a function of surface area of solid catalysts employed (**a**), and Brönsted sites of the zeolites (**b**).

On the other hand, metallic copper has an increased catalytic action comparing with the behavior of iron wires. This could be well explained taking into account the different intrinsic physicochemical characteristics that both metals have. For instance, while the electronegativity for copper and iron are very similar (1.9 and 1.8 respectively, Pauling scale), the electron affinity (-118 kJmol^{-1} and -16 kJmol^{-1}, respectively) and the thermal conductivity (3.81 Wcm^{-1}K^{-1} and 0.56 Wcm^{-1}K^{-1} at 573.2 K, respectively) are quite different.[24] Blazsó and Jakab investigated the effect of metals and metal oxides on the thermal decomposition processes of PVC.[25] They propose that the dechlorination process begins when the C–Cl bonds are loosened due to the attraction of the chlorine by the metal, chlorine driven away from the carbon allow to the thermal decomposition process yield aromatic hydrocarbons. In our case, we propose that dechlorination and decomposition processes occur with a better performance over copper

than iron due to combination of these two properties that make to these materials have a very different behavior. To higher electron affinity and thermal conductivity of copper, major interaction with the substrate and better energy transfer (heat) toward the C-Cl bond that is stretching occur, **scheme 3**.

In addition, it is important to note that one of the main by-product obtained in the organic phase for both metals is the 2-dechlorinated product as it was demonstrated for Blazsó and Jakab in the thermolysis of PCV.[25]
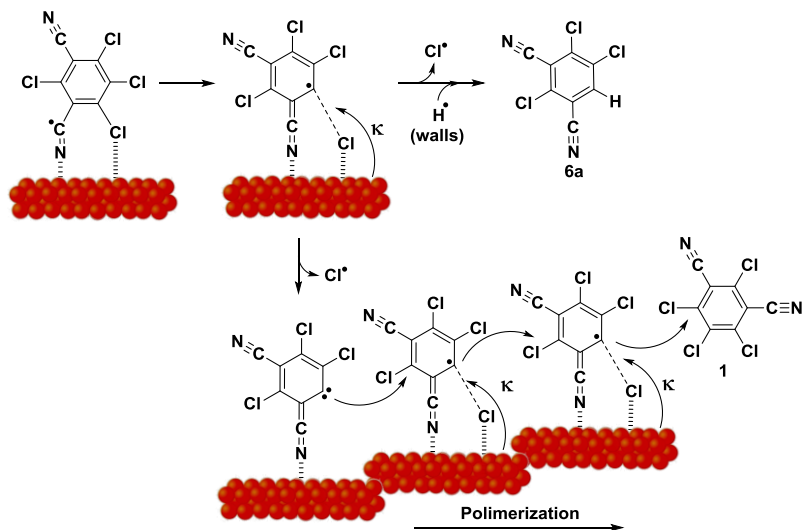
Scheme 3. Proposed mechanism of heterogeneous pyrolysis of **1** over metal surfaces (K: thermal conductivity).

3.4. Pyrolysis of CT derivatives

The mass remaining from homogeneous as well as heterogeneous pyrolyses of **2-5** at 400ºC is presented in **table 4**. For all derivatives, the homogeneous pyrolyses showed a rather small decomposition with correspondingly high masses remaining. Nevertheless, when the thermolyses were performed in the presence of H-Y, high decomposition were generally observed, and particularly, the most surprising result was observed with the aliphatic derivative **2** that was completely decomposed and no mass could be recovered. In this case, an important amount of coke, easily visible by the dark color that the catalyst took, was formed and retained in the zeolite. Besides, gaseous species were produced as proved by FTIR that showed the formation of hydrogen chloride, methane, carbon dioxide and carbon monoxide, **figure 10**. The pyrolysis crude without catalyst, was analyzed *via* GC-MS where the main degradation pathway was the dealkylation of **2**, rendering a primary amine, see **scheme 4** and also MS presented in the **figures S37-38** in the Supplementary Material.

Table 4. Mass remaining (%w/w) in the pyrolysis of **2-5** at 400ºC.

Compound	Time (min)	Homogeneous (%)	H-Y (%)
2	20	94.2	0.03
3	20	78.9	45.3
	30	76.7	34.5
4	20	94.4	51.6
5	20	98.0	52.7
	30	69.0	14.1

14
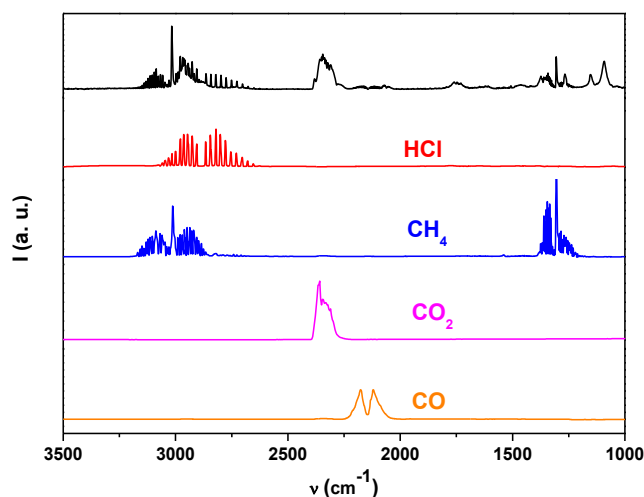
Figure 10. FTIR spectrum of the thermolysis of **2** and characterization of the gas products.
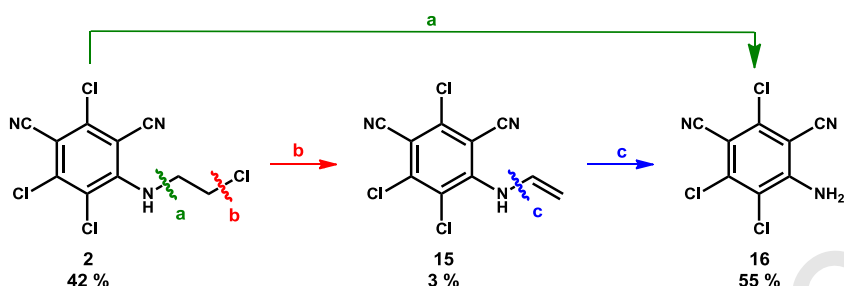
Scheme 4. Pyrolysis products of **2** at 400⁰C in the homogeneous phase.

For the aromatic compounds (**3-5**), the same product (**17**) was observed (see MS presented in **figure S39** in the Supplementary Material). The mechanism for its formation is proposed in **scheme 5**. We believe that the first step is the formation of a well-known aza-vinyl carbene **i** *via* hydrogen chloride elimination (path A).[26] The next step (B) would be the intra molecular insertion of this carbene to give the unstable azirine **ii** which, after the loss of the aryl moiety, yields intermediate **iii** (C). Subsequent, this very unstable intermediate suffers a ring opening reaction to produce the elimination of a chlorine atom (D), ending in the formation of the nitrene **iv** which in turn should dimerize to form the final dihydrophenazine **17**. Nevertheless, we are not able to discard the direct loss of Cl-Ar (F) to form the nitrene **iv**, instead of the step by step route (A-C). Should this be the case, the Cl-Ar product (**18**) would have been detected in high yields, instead of traces as it was observed. In terms of yields of reaction, for the aliphatic derivative, the yield was extremely low and only traces of **17** were found. For the aromatic family, the yield was scarce when no substitution on the phenyl ring was present (5.7%), with good yield for chlorine as substituent (75.9%). The other halogen involved, Br, produced a very low yield (15.2%) probably due to the lability of the C-Br bond that could break before the nitrene formation.

15
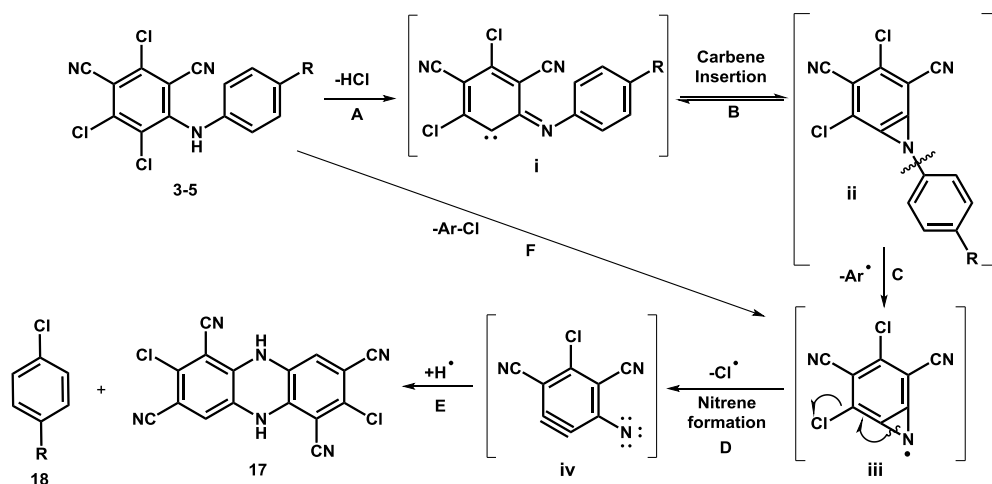
Scheme 5. Proposed mechanism for gas phase pyrolysis of **3-5**.

4. Conclusions

The results obtained in the present work reflect the performance of heterogeneous catalysis in the degradation of chlorothalonil and derivatives. The zeolites ZSM-11 and Y have shown a good correspondence between the catalytic activities and their acidic and structural properties.

H-Y did produce degradation of **1** within its channels, while H-ZSM-11 worked mainly as an adsorbent of **1**. This behavior can be attributed to diffusional restrictions related to its microporous structure (pores defined by ten member rings) that hinder the access of molecules to the internal acid sites. On the contrary H-Y, with higher accessibility to their active sites (pores defined by twelve member rings) was more active. M-Y zeolites showed a decrease in reactivity compared to the H-Y. This statement agrees with the determinations presented on **table 2** (Brönsted acidic sites), where Cu-Y present the lowest value and H-Y the highest. Besides, copper surface presented the highest decomposition of **1** while iron surface presented the lowest one, probably due to the specific properties that produce a very different behavior of these metals.

Chlorothalonil derivatives were prepared and their pyrolysis were explored. **2** presented dealkylation to yield **16** in the homogeneous pyrolysis, while the heterogeneous one produced great amounts of hydrogen chloride, methane, carbon dioxide, carbon monoxide and carbonaceous residues retained within the zeolites channels. On the other hand, **3-5** generated the same product (**17**).

References

1-A. Sakkas, D.A. Lambropoulou, T.A. Albanis, Study of chlorothalonil photodegradation in natural waters and in the presence of humic substances, Chemosphere 48 (2002) 939-945. https://doi.org/10.1016/S0045-6535(02)00121-2

2-P.Y. Caux, R.A. Kent, G.T. Fan, G.L. Stephenson, Environmental fate and effects of chlorothalonil: A Canadian perspective, Crit. Rev. Environ. Sci. Technol. 26 (1996) 45-93. https://doi.org/10.1080/10643389609388486

3-M.V. Cooke, M.B. Oviedo, W.J. Peláez, G.A. Argüello, UV characterization and photodegradation mechanism of the fungicide chlorothalonil in the presence and absence of oxygen, Chemosphere 187 (2017) 156-162. https://doi.org/10.1016/j.chemosphere.2017.08.111

4-L. Baoyu, X. Kaihong, C.O. Su, S. Dalei, F. Yanxiong, X. Hongxia, Direct synthesis of hierarchical USY zeolite for retardation of catalyst deactivation, Chemical Engineering Science 153 (2016) 374-381. https://doi.org/10.1016/j.ces.2016.07.041

5-J. Perez-Ramirez, C.H. Christensen, K. Egeblad, C.H. Christensen, J.C. Groen, Hierarchical zeolites: enhanced utilization of microporous crystal sin catalysis by advances in materials design, Chem. Soc. Rev. 37 (2008) 2530-2542. https://doi.org/10.1039/B809030K

6-M.S. Renzini, U. Sedran, L.B. Pierella, H-ZSM-11 and Zn-ZSM-11 zeolites and their applications in the catalytic transformation of LDPE, J. Anal. Appl. Pyrolysis 86 (2009) 215–220. https://doi.org/10.1016/j.jaap.2009.06.008

7-M. Guisnet, P. Magnoux, Organic Chemistry of Coke Formation, Appl. Catal., A General 212 (2001) 83-96. https://doi.org/10.1016/S0926-860X(00)00845-0

8-https://pubchem.ncbi.nlm.nih.gov/compound/15910

9-L.P. Shi, K.M. Jiang, Y. Jin, Y.H. Tao, K. Li, X.H. Wang, J. Lin, Synthesis and antimicrobial activity of polyhalobenzonitrile quinazolin-4(3H)-one derivatives, Bioorg. Med. Chem. Lett. 23 (2013) 5958-5963. https://doi.org/10.1016/j.bmcl.2013.08.068

10-Chu, P. U.S. Patent No. 3,709,979. Washington, DC: U.S. Patent and Trademark Office. 9 Jan. 1973. https://patentimages.storage.googleapis.com/49/12/d2/1f69d352997e1e/US3709979.pdf

11-C.A. Emeis, Determination of Integrated Molar Extinction Coefficients for Infrared Absorption Bands of Pyridine Adsorbed on Solid Acid Catalysts, J. Catal. 141 (1993) 347-354. https://doi.org/10.1006/jcat.1993.1145

12-G. Busca, The surface acidity of solid oxides and its characterization by IR spectroscopic methods. An attempt at systematization, Phys. Chem. Chem. Phys. 1 (1999) 723-736. https://doi.org/10.1039/A808366E

13-K. Rhee, U. Rao, J. Stencel, G. Melson, J. Crawford, Supported transition metal compounds: Infrared studies on the acidity of Co/ZSM-5 and Fe/ZSM-5 catalysts, Zeolites 3 (1983) 337-343. https://doi.org/10.1016/0144-2449(83)90179-3

14-R. Borade, A. Sayari, A. Adnot, S. Kaliaguine, Characterization of acidity in ZSM-5 zeolites: an x-ray photoelectron and IR spectroscopy study, J. Phys. Chem. 94 (1990) 5989–5994. https://pubs.acs.org/doi/10.1021/j100378a068

15-S. Singh, C. Wu, P.T. Williams, Pyrolysis of waste materials using TGA-MS and TGA-FTIR as complementary characterisation techniques, J. Anal. Appl. Pyrolysis 94 (2021) 99-107. https://doi.org/10.1016/j.jaap.2011.11.011

16-H. Cerqueira, G. Caeiro, L. Costa, F. Ramôa Ribeiro, Deactivation of FCC Catalysts, J. Mol. Catal. A: Chem. 292 (2008) 1-13. https://doi.org/10.1016/j.molcata.2008.06.014

17-M.S. Renzini, L.C. Lerici, U. Sedran, L.B. Pierella, Stability of ZSM-11 and BETA zeolites during the catalytic cracking of low-density polyethylene, J. Anal. Appl. Pyrolysis 92 (2011) 450-455. https://doi.org/10.1016/j.jaap.2011.08.008

18-Y.H. Lin, P.N. Sharratt, A.A. Garforth, J. Dwyer, Deactivation of US-Y zeolite by coke formation during the catalytic pyrolysis of high density polyethylene, Thermochim. Acta 294 (1997) 45-50. https://doi.org/10.1016/S0040-6031(96)03141-3

19- B. Paweewan, Patrick J. Barrie, Lynn F. Gladden, Coking and deactivation during n-hexane cracking in ultrastable zeolite Y, Applied Catalysis A: General 185 (1999) 259–268. https://doi.org/10.1016/S0926-860X(99)00143-X

20-J.B. Parise, D.R. Corbin, L. Abrams, D.E. Cox, Structure of dealuminated Linde Y-zeolite; $Si_{139.7}Al_{52.3}O_{384}$ and $Si_{173.1}Al_{18.9}O_{384}$: presence of nonframework Al species, Acta Crystallographica Section C. 40:9 (1984) 1493-1497. https://doi.org/10.1107/S0108270184008490

21-A.J. Pepino, W.J. Peláez, G.A. Argüello, From new simple aliphatic to aromatic heterocycles built from 2-chloroethylisocyanate, J. Anal. App. Pyrol., 105 (2014), 49-54. https://doi.org/10.1016/j.jaap.2013.10.003

22- Alexander R. Stanton, Kristiina Lisa, Matthew M. Yung, Kimberly A. Magrini, Catalytic fast pyrolysis with metal-modified ZSM-5 catalysts in inert and hydrogen atmospheres, Journal of Analytical and Applied Pyrolysis 135 (2018) 199–208. https://doi.org/10.1016/j.jaap.2018.09.002

23-Lei Ji, Antoine Hervier, Michel Sablier, Study on the pyrolysis of polyethylene in the presence of iron and copper chlorides, Chemosphere 65 (2006) 1120–1130. https://doi.org/10.1016/j.chemosphere.2006.04.029

24-C.Y. Ho, R. W. Powell, P. E. Liley, Journal of Physical and Chemical Reference Data, 3, suppl.1 (1974), Thermal conductivity of elements: a comprehensive review. https://srd.nist.gov/JPCRD/jpcrdS1Vol3.pdf

25-M. Blazsó, E. Jakab, Journal of Analytical and Applied Pyrolysis 49 (1999) 125–143. https://doi.org/10.1016/S0165-2370(98)00123-5

26-R.A. Aitken, Y. Boubalouta, Chapter Two - Recent Advances in the Synthesis of Heterocyclic Compounds Using Flash Vacuum Pyrolysis, E.F.V. Scriven, C.A. Ramsden (Eds.), Advances in Heterocyclic Chemistry, 115 (2015), 93-150. https://doi.org/10.1016/bs.aihch.2015.03.002